Article

Research and Evaluation of a New Structural Damage Identification Method Based on a Refined Genetic Algorithm

Yuantian Qin *[ID], Zhehang Yin and Jiahao Ma

College of Astronautics, Nanjing University of Aeronautics and Astronautics, Nanjing 210016, China; yinzhehang@nuaa.edu.cn (Z.Y.); majiahao51@163.com (J.M.)
* Correspondence: qinyt@nuaa.edu.cn

Abstract: In order to solve the problem of structural damage location and degree identification, the weighted mean of vectors algorithm (INFO), a high-performance optimization algorithm, was first introduced to identify structural damage. By comparison with the refined genetic algorithm (RGA), the accuracy and advantages of INFO are analyzed and evaluated. An objective function is constructed by combining the dynamic response transfer ratio without modal analysis. The INFO and RGA algorithms are used to optimize the objective function for damage identification. The simulation results verify the effectiveness of the three damage identification methods. The results show that the identification effect of the INFO algorithm can reach nearly 100% without noise influence, and the anti-noise ability is the strongest. Among the three algorithms, the damage identification accuracy of the INFO algorithm is the highest, followed by the RGA algorithm and the GA algorithm.

1. Introduction

As more and more large-scale space engineering structures are put into use, it has become a hot topic for engineers and scholars in various countries to establish a matching structural health monitoring system for all-around safety assurance, and one of the most important aspects is how to effectively identify damage to space structures, including damage localization and quantitative analysis of the damage degree.

Damage identification based on the difference in the dynamic properties of the structure before and after damage has been a hotspot of concern in the engineering community. Related technology applications in the field of engineering are numerous; the most famous use of the technology is the 101 building in Taipei, China [1]. This type of strategy determines the location and extent of damage by evaluating the correlation of the dynamic parameters of the healthy and damaged structure, which is essentially an inverse problem, and the finite element model updating technique is often applied to solve this type of inverse problem.

Damage identification methods based on finite element model updating can transform the damage identification problem into a constrained optimization problem, which generally starts with the establishment of an objective function for evaluating the structural relevance of health and damage, and this is subsequently solved using an optimization algorithm to find an optimal solution. However, traditional optimization algorithms, such as the most rapid descent method and the conjugate gradient method, are not only slow to converge but also prone to fall into local optima. Therefore, it is significant for damage identification field to develop and search for more powerful optimization algorithms.

With the rapid development of intelligent optimization algorithms in recent times, more and more scientists have studied this in depth and used it to solve optimization problems in damage identification. Qian, C. Y. et al. [2] utilized an improved cuckoo algorithm, which is an algorithm combining frequency and vibration factors that has a strong global search ability but needs to search parameters manually, for damage identification in benchmark frames with significant results. Vaez, S. R. H. et al. [3] proposed a hybrid genetic and particle swarm algorithm for

damage identification in damaged thin-plate models and achieved good results; the algorithm was found to have strong search capabilities and a fast convergence speed, although it takes a long time for a single iteration. Wan, Z. H. et al. [4] proposed a two-stage damage identification method based on the augmented whale algorithm to successfully identify multiple occurrences of damage in simply supported beams with thin plates; this is a new algorithm with strong search capabilities and robustness, although the accuracy is not as good as the best algorithms. Mohan, S. C. et al. [5] successfully localized and quantified the damage in beams and planar frames using a damage detection technique based on the frequency response function and particle swarm algorithm, but some evaluations of the performance of this technology were missing. Miguel, L. F. F. et al. [6] proposed a hybrid stochastic/deterministic optimization algorithm for damage identification, which is more accurate and efficient in identifying damage when compared with genetic, harmonic, and particle swarm algorithms. Ding, Z. H. et al. [7] proposed a damage identification method based on the artificial bee colony algorithm with a hybrid search strategy and modal data and successfully identified damage in a truss model and a plate model; they were also able to achieve a balance between global and local searches to avoid falling into an local optimal solution with dependencies on parameter selection. Pan, C. D. et al. [8] proposed a damage identification method based on a hybrid adaptive firefly algorithm and verified the validity of the proposed method using a two-story rigid frame structure and beam model, but the results showed that the performance improvement of this algorithm was not obvious compared with other algorithms. Chen, Z. P. et al. [9] embedded the Nelder–Mead algorithm into a particle swarm algorithm to obtain a hybrid particle swarm algorithm and used it for damage identification, and they verified the effectiveness and superiority of the method through the numerical simulation of simply supported beams as well as experiments on rectangular cross-section steel beams; however, because PSO required a lot of calculations, the calculation time was greatly extended. Guilherme, F. G. et al. [10] proposed an optimization algorithm based on sunflower motion and successfully identified damage in composite laminates by this algorithm. It tracks the sun's movement patterns and fertilization strategies by simulating sunflowers. The algorithm performed the global search by updating the position and limiting the maximum stride length. The results show that SFO had good accuracy and calculation speed performance in damage identification. Alkayem, N. F. et al. [11] proposed a damage identification method based on the social swarm algorithm, modal strain energy, and modal vibrational curvature and verified the effectiveness of the method by a numerical simulation without noise analysis or a performance evaluation. Huang, M. S. et al. [12] proposed a damage identification method based on the modal frequency strain energy assurance criterion, modal flexibility, and enhanced moth flame optimization algorithm and verified the effectiveness of the method using simply supported beams and triple-shear frame experiments, which showed that this method had good performance in simplicity and convergence speed, although the global search ability was not outstanding, and there was a lack of suitable reference comparisons. Minh, H. L. et al. [13] proposed an augmented particle swarm algorithm for solving the damage identification problem and successfully applied the method to the damage identification of power transmission towers; however, the structure of transmission towers has its particularity, so the universality of this method had not been verified. Li, X. L. et al. [14] proposed a multi-component particle swarm algorithm with cooperative learning for damage identification, which fuses four particle swarm algorithm variants to build a pool of strategies, and the numerical simulation results show that the algorithm possesses higher accuracy in damage identification compared with a single variant and other algorithms; however, it comes at the cost of a huge increase in computing time. Li, Y. F. et al. [15] proposed a hybrid K-clustering mean optimization algorithm and used it for the identification of damage in small experimental dams, and the results show that this algorithm has high accuracy and computational efficiency for the identification of large and complex structures. Thanh, S. T. et al. [16] proposed the Goby joint search algorithm and used it for damage identification in Guangzhou Tower; the results show that this algorithm has higher damage identification accuracy compared with GAs, genetic particle swarm hybrid algorithms and others. Muhammad, I. S. et al. [17] proposed a damage identification method based on a hybrid YUKI-ANN algorithm with a modal strain energy

change ratio and successfully applied it for damage identification in plywood, but there was no systematic evaluation of this method.

In previous research, the application of INFO [18] in damage identification has been relatively rare. The INFO algorithm is an efficient optimization tool that effectively explores the solution space and quickly converges to the global optimum through a weighted average method, while also having an improved mechanism to enhance its search capabilities and accuracy. As a relatively new algorithm, INFO has not been accurately evaluated for its potential application, performance, and advantages and disadvantages in identifying the direction of loss. In addition, most of the literature only carried out a simple application of the adopted method and did not refer to existing methods for a detailed evaluation and guidance of the adopted algorithms.

In this paper, a high-performance optimization algorithm—INFO—is introduced to establish an objective function. An objective function based on the dynamic response transfer ratio is established, and the weighting factor calculated by the damage classification is used to balance the sensitivity of each part of the function to damage. Next, the RGA is obtained by adding an improved non-uniform mutation method, improved mutation rate method, and cross-rate change method [19] to the genetic algorithm. The RGA algorithm is then used as a reference to evaluate the effect of INFO. Finally, taking simply supported beams and cantilever plates as objects, GA, RGA, and INFO are utilized to identify a variety of damage cases under different levels of noises and different spacings of frequency-point pickup points to verify the effectiveness of the methods and to compare the damage identification effect of the algorithms.

2. Weighted Mean of Vectors

INFO is a new type of intelligent algorithm proposed by Dr. Ahmadianfar et al. in 2022. The algorithm applies the improved weighted mean idea to the entity structure and updates the solution vector through three core steps: updating the rules, combining the vectors, and performing a local search. The algorithm has characteristics of high speed and high accuracy and is simple, effective and robust. At the same time, it can effectively avoid the local optimal situation. Most importantly, it is a sufficiently novel and open-source algorithm to make it a suitable reference algorithm. The specific implementation process is described as follows (Figure 1 depicts the flow of the INFO).
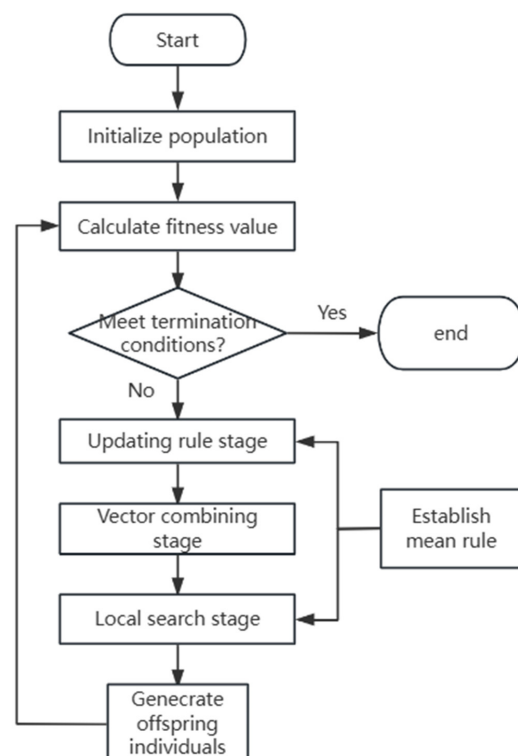

Figure 1. Flow of the INFO.

2.1. Updating Rule Stage

INFO's updating rule operator uses the weighted mean of the vectors to create new vectors and performs an efficient global search in this way. Firstly, INFO has to randomly select three difference vectors from all the solution vectors of each generation to calculate the vector-weighted mean value $\boldsymbol{WM1}^{it}$; at the same time, it selects the best-, better-, and worst-solution vectors of the total solution vectors to calculate the vector-weighted mean value $\boldsymbol{WM2}^{it}$. These can be expressed, respectively, as

$$\boldsymbol{WM1}^{it} = sc \cdot \frac{rh_1 \cdot \left(\boldsymbol{u}_{gx}^{it} - \boldsymbol{u}_{gy}^{it}\right) + rh_2 \cdot \left(\boldsymbol{u}_{gi}^{it} - \boldsymbol{u}_{gz}^{it}\right) + rh_3 \cdot \left(\boldsymbol{u}_{gy}^{it} - \boldsymbol{u}_{gz}^{it}\right)}{rh_1 + rh_2 + rh_3 + ep} + ep \cdot rand_1 \cdot \boldsymbol{oe} \quad (1)$$

$$\boldsymbol{WM2}^{it} = sc \cdot \frac{rh_4 \cdot \left(\boldsymbol{u}_{bs}^{it} - \boldsymbol{u}_{bt}^{it}\right) + rh_5 \cdot \left(\boldsymbol{u}_{bs}^{it} - \boldsymbol{u}_{w}^{it}\right) + rh_6 \cdot \left(\boldsymbol{u}_{bt}^{it} - \boldsymbol{u}_{ws}^{it}\right)}{rh_4 + rh_5 + rh_6 + ep} + ep \cdot rand_2 \cdot \boldsymbol{oe} \quad (2)$$

where

$$rh_1 = \cos\left(\mathrm{obj}\left(\boldsymbol{u}_{gx}^{it}\right) - \mathrm{obj}\left(\boldsymbol{u}_{gy}^{it}\right) + \pi\right) \cdot \exp\left(-\left|\frac{\mathrm{obj}\left(\boldsymbol{u}_{gx}^{it}\right) - \mathrm{obj}\left(\boldsymbol{u}_{gy}^{it}\right)}{\max\left(\mathrm{obj}\left(\boldsymbol{u}_{gx}^{it}\right), \mathrm{obj}\left(\boldsymbol{u}_{gy}^{it}\right), \mathrm{obj}\left(\boldsymbol{u}_{gz}^{it}\right)\right)}\right|\right)$$

$$rh_2 = \cos\left(\mathrm{obj}\left(\boldsymbol{u}_{gx}^{it}\right) - \mathrm{obj}\left(\boldsymbol{u}_{gz}^{it}\right) + \pi\right) \cdot \exp\left(-\left|\frac{\mathrm{obj}\left(\boldsymbol{u}_{gx}^{it}\right) - \mathrm{obj}\left(\boldsymbol{u}_{gz}^{it}\right)}{\max\left(\mathrm{obj}\left(\boldsymbol{u}_{gx}^{it}\right), \mathrm{obj}\left(\boldsymbol{u}_{gy}^{it}\right), \mathrm{obj}\left(\boldsymbol{u}_{gz}^{it}\right)\right)}\right|\right)$$

$$rh_3 = \cos\left(\mathrm{obj}\left(\boldsymbol{u}_{gy}^{it}\right) - \mathrm{obj}\left(\boldsymbol{u}_{gz}^{it}\right) + \pi\right) \cdot \exp\left(-\left|\frac{\mathrm{obj}\left(\boldsymbol{u}_{gy}^{it}\right) - \mathrm{obj}\left(\boldsymbol{u}_{gz}^{it}\right)}{\max\left(\mathrm{obj}\left(\boldsymbol{u}_{gx}^{it}\right), \mathrm{obj}\left(\boldsymbol{u}_{gy}^{it}\right), \mathrm{obj}\left(\boldsymbol{u}_{gz}^{it}\right)\right)}\right|\right)$$

$$rh_4 = \cos\left(\mathrm{obj}\left(\boldsymbol{u}_{gs}^{it}\right) - \mathrm{obj}\left(\boldsymbol{u}_{gt}^{it}\right) + \pi\right) \cdot \exp\left(-\left|\frac{\mathrm{obj}\left(\boldsymbol{u}_{gs}^{it}\right) - \mathrm{obj}\left(\boldsymbol{u}_{gt}^{it}\right)}{obj\left(\boldsymbol{u}_{ws}^{it}\right)}\right|\right)$$

$$rh_5 = \cos\left(\mathrm{obj}\left(\boldsymbol{u}_{gs}^{it}\right) - \mathrm{obj}(\boldsymbol{u}_{ws}^{it}) + \pi\right) \cdot \exp\left(-\left|\frac{\mathrm{obj}\left(\boldsymbol{u}_{bs}^{it}\right) - \mathrm{obj}\left(\boldsymbol{u}_{ws}^{it}\right)}{obj\left(\boldsymbol{u}_{ws}^{it}\right)}\right|\right)$$

$$rh_6 = \cos\left(\mathrm{obj}(\boldsymbol{u}_{bt}^{it}) - \mathrm{obj}(\boldsymbol{u}_{ws}^{it}) + \pi\right) \cdot \exp\left(-\left|\frac{\mathrm{obj}\left(\boldsymbol{u}_{bt}^{it}\right) - \mathrm{obj}\left(\boldsymbol{u}_{ws}^{it}\right)}{obj\left(\boldsymbol{u}_{ws}^{it}\right)}\right|\right)$$

In the above expressions, $\mathrm{obj}(\boldsymbol{u})$ is the value of the objective function, and $\boldsymbol{u}_{gx}^{it}$, $\boldsymbol{u}_{gy}^{it}$, and $\boldsymbol{u}_{gz}^{it}$ are individuals in the itth generation. The variables gx, gy, and gz are different integers randomly chosen from the range $[0, 1]$; NP is the population size; ep is an infinitesimal constant; $rand1$ and $rand2$ are random numbers within the range $[0, 1]$; $\boldsymbol{oe}$ is a vector whose all elements are 1; $\boldsymbol{u}_{bs}^{it}$, $\boldsymbol{u}_{bt}^{it}$, and $\boldsymbol{u}_{ws}^{it}$ are the best, better, and worst individuals in the itth generation, respectively; and sc is a scaling factor, which can be expressed as follows:

$$sc = (4\mathrm{rand}_3 - 2) \cdot \exp\left(-\frac{4it}{\mathrm{Maxit}}\right) \quad (3)$$

where $rand_3$ is a random number within the range $[0, 1]$, and Maxit is the maximum number of evolutionary generations.

Next, INFO uses $\boldsymbol{WM1}^{it}$ and $\boldsymbol{WM2}^{it}$ to construct the MeanRule, which can be expressed as follows:

$$\mathrm{MeanRule} = \theta \cdot \boldsymbol{WM}^t + (1 - \theta) \cdot \boldsymbol{WM2}^2 \quad (4)$$

where θ is a random number within the range $[0, 0.5]$. Finally, to further improve the global search capability of the algorithm, an additional convergence acceleration module is added, which makes full use of the optimal solution vectors in each generation to change the current solution vectors in the search space. Therefore, the final update rule formula for INFO is expressed as follows:

$$\boldsymbol{cz1}_{nu}^{it} = \begin{cases} \boldsymbol{u}_{nu}^{it} + \sigma \cdot \mathrm{MeanRule} + \mathrm{randn}_1 \cdot \frac{\left(\boldsymbol{u}_{bs}^{it} - \boldsymbol{u}_{gx}^{it}\right)}{\left(\mathrm{obj}\left(\boldsymbol{u}_{bs}^{it}\right) - obj\left(\boldsymbol{u}_{gx}^{it}\right) + 1\right)} & \mathrm{rand}_4 < 0.5 \\[4mm] \boldsymbol{u}_{gx}^{it} + \sigma \cdot \mathrm{MeanRule} + \mathrm{randn}_2 \cdot \frac{\left(\boldsymbol{u}_{gy}^{it} - \boldsymbol{u}_{gz}^{it}\right)}{\left(\mathrm{obj}\left(\boldsymbol{u}_{gy}^{it}\right) - obj\left(\boldsymbol{u}_{gz}^{it}\right) + 1\right)} & \mathrm{rand}_4 \geq 0.5 \end{cases} \quad (5)$$

$$cz2^{it}_{nu} = \begin{cases} u^{it}_{bs} + \sigma \cdot \text{MeanRule} + \text{randn}_3 \cdot \frac{\left(u^{it}_{gx} - u^{it}_{gy}\right)}{\left(\text{obj}\left(u^{it}_{gx}\right) - obj\left(u^{it}_{gy}\right) + 1\right)} & \text{rand}_4 < 0.5 \\ u^{it}_{bt} + \sigma \cdot \text{MeanRule} + \text{randn}_4 \cdot \frac{\left(u^{it}_{gx} - u^{it}_{gy}\right)}{\left(\text{obj}\left(u^{it}_{gx}\right) - obj\left(u^{it}_{gy}\right) + 1\right)} & \text{rand}_4 \geq 0.5 \end{cases} \tag{6}$$

where $cz1^{it}_{nu}$ and $cz2^{it}_{nu}$ are the new solution vectors of the *it*th generation; $nu = 1, 2, \ldots, NP$ and $nu \neq gx \neq gy \neq yz$; and u^{it}_{nu} represents any random individual except u^{it}_{gx}, u^{it}_{gy}, and u^{it}_{gz} in the *it*th generation. randn_4 is a random number within the range $[0, 1]$, and randn_1, randn_2, randn_3, and randn_4 are standard normally distributed random numbers. σ is the scaling factor, which can be expressed as follows:

$$\sigma = (4\text{rand}_5 - 2) \cdot \exp\left(-\frac{4it}{\text{Maxit}}\right) \tag{7}$$

where rand_5 is a random number within the range $[0, 1]$.

2.2. Vector Combining Stage

To improve the local search capability of INFO, the solution vectors $cz1^{it}_{nu}$ and $cz2^{it}_{nu}$ computed in the updating rule stage are combined to generate a new solution vector cv^{it}_{nu}, which can be expressed as follows:

$$cv^{it}_{nu} = \begin{cases} cz1^{it}_{nu} + ns \cdot \left|cz1^{it}_{nu} - cz2^{it}_{nu}\right| & \text{rand}_6 < 0.5 \text{ and } \text{rand}_7 < 0.5 \\ cz2^{it}_{nu} + ns \cdot \left|cz1^{it}_{nu} - cz2^{it}_{nu}\right| & \text{rand}_6 < 0.5 \text{ and } \text{rand}_7 \geq 0.5 \\ u^{it}_{nu} & \text{rand}_6 \geq 0.5 \end{cases} \tag{8}$$

where $ns = 0.05 \, \text{randn}_5$, randn_5 is a standard normally distributed random number, and randn_6 and randn_7 are random numbers within the range $[0, 1]$.

2.3. Local Search Stage

The local search stage will create a new solution vector cvs^{it} based on the mean rule, which further enhances the local search capability of INFO, and the specific implementation formula can be expressed as:

$$cvs^{it} = \begin{cases} u^{it}_{bs} + \text{randn}_6 \cdot \left(\text{MeanRule} + \text{randn}_7 \cdot \left(u^{it}_{bs} - u^{it}_{gx}\right)\right) & \text{rand}_8 < 0.5 \text{ and } \text{rand}_9 < 0.5 \\ u^{it}_{md} + \text{randn}_8 \cdot \left(\text{MeanRule} + \text{randn}_9 \cdot \left(vs_1 \cdot u^{it}_{bs} - vs_2 u^{it}_{md}\right)\right) & \text{rand}_8 < 0.5 \text{ and } \text{rand}_9 \geq 0.5 \end{cases} \tag{9}$$

where

$$u^{i}_{md} = \phi \cdot \frac{\left(u^{it}_{gx} + u^{it}_{gy} + u^{it}_{gz}\right)}{3} + (1 - \phi) \cdot \left(\phi \cdot u^{it}_{bt} + (1 - \phi) \cdot u^{it}_{bs}\right)$$

$$vs_1 = \begin{cases} 2\text{rand}_{10} & \eta > 0.5 \\ 1 & \eta \leq 0.5 \end{cases}, \quad vs_2 = \begin{cases} \text{rand}_{11} & \eta > 0.5 \\ 1 & \eta \leq 0.5 \end{cases}$$

where ϕ, rand_8, rand_9, η, rand_{10}, and rand_{11} are random numbers within the range $[0, 1]$, and rand_6, rand_7, rand_8, and rand_9 are standard normally distributed random numbers.

3. Genetic Algorithm Refinement

The GA has strong global search performance and high efficiency and robustness, but subsequent studies have also shown that the GA performs poorly in local searches, and the algorithm itself is prone to immature, slow convergence, degradation and other problems [20]. To address these problems, this paper improves the mutation operator, crossover, and mutation rate. The operations of the RGA are as follows (Figure 2 depicts the flow of the RGA).
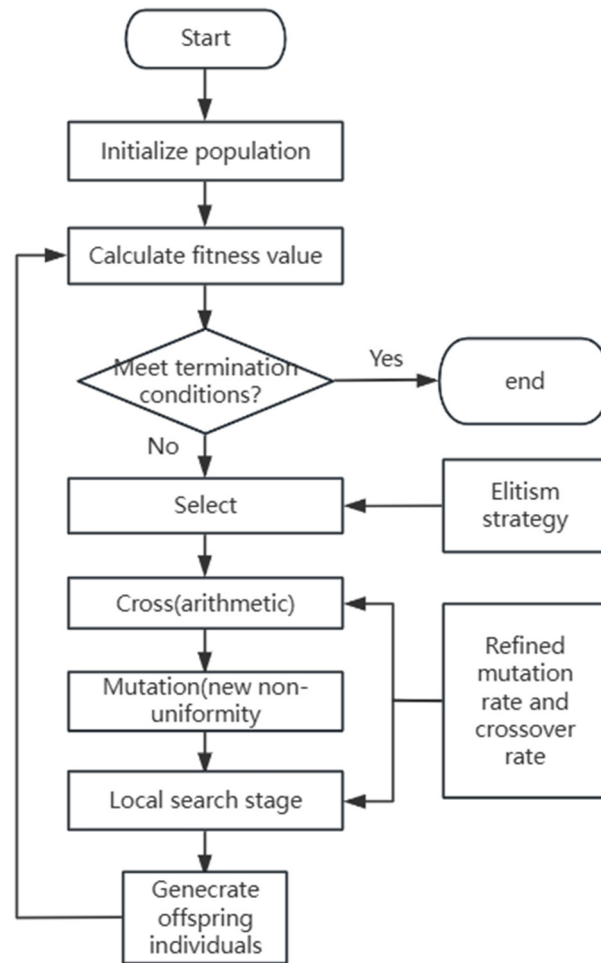
Figure 2. Flow of the RGA.

3.1. Selection and Crossover

The selection operation in the paper adopts roulette wheel selection, while adding the elitism retention strategy. Roulette wheel selection and elitism are common operations and strategies in GAs. The roulette selection method is a selection process in which the probability of each individual being selected is proportional to its fitness. The higher the individual's fitness, the greater the chance of being selected. This approach mimics the "survival of the fittest" principle of natural selection. The elite retention strategy refers to the fact that in each generation of the population, a certain number of the best individuals (elite) are copied directly to the next generation to ensure that good genes are not lost. This helps the algorithm maintain the good solutions it has already found and may avoid premature convergence. The crossover operation adopts arithmetic crossover, which selects any two bodies in the parent generation for linear combination to produce a new individual, which can be expressed as:

$$\begin{cases} G_{A1}^{gt+1} = \lambda \cdot G_{A2}^{gt} + (1-\lambda) \cdot G_{A1}^{gt} \\ G_{A2}^{gt+1} = \lambda \cdot G_{A1}^{gt} + (1-\lambda) \cdot G_{A2}^{gt} \end{cases} \tag{10}$$

where $A1$ and $A2$ represent two different individuals, G_{A1}^{gt} and G_{A2}^{gt} are the individuals of the gtth generation, G_{A1}^{gt+1} and G_{A2}^{gt+1} are the individuals of the $gt+1$th generation, and λ is a random number within the range [0, 1]. To ensure that the crossover individuals do not exceed the specified range, a bounding judgment is added. Figure 3 displays the arithmetic crossover.

Figure 3. Arithmetic crossover.

3.2. Mutation

In this paper, the RGA uses a modified non-uniform mutation approach, which is a mutation operation that allows large variations in the early stages of the algorithm to facilitate a global search while reducing the amplitude of variation in the later stages to refine the search and find more precise solutions, randomly selecting individuals and generating a non-uniform perturbation to them that varies according to the number of evolutionary generations to improve the algorithm's ability to search for the focal region. After processing and calculation, the improvement can be expressed as

$$
G_{\text{new}}^{gt} = \begin{cases} G_{\text{old}}^{gt} + G_{\text{old}}^{gt} \cdot \lambda_1 \cdot \left(1 - (gt/Maxg)^{0.84}\right)^{tb} & \lambda_2 \geq 0.5 \\ G_{\text{old}}^{gt} - G_{\text{old}}^{gt} \cdot \lambda_1 \cdot \left(1 - (gt/Maxg)^{0.84}\right)^{tb} & \lambda_2 < 0.5 \end{cases} \tag{11}
$$

where G_{old}^{gt} and G_{new}^{gt} denote the unmutated and mutated individuals in the gtth generation, respectively; $Maxg$ is the maximum number of generations; λ_1 and λ_2 are random numbers within the range $[0, 1]$; and tb is a suitable perturbation parameter, which is taken as 3.7 in this paper. To ensure that the new individuals, after mutation, will not exceed the specified range, this step also requires boundary judgment.

3.3. Mutation Rate and Crossover Rate

In this paper, the RGA adopts a modified crossover rate and mutation rate change method, in which, on the one hand, the exponential function is used to increase the strength of crossover and mutation to increase the diversity of the population so as not to let the population tend to a single dominant individual and fall into the local optimum, and, on the other hand, the good individuals will be retained due to the small crossover rate and mutation rate, and the poor individuals will disappear rapidly due to the large mutation rate and crossover rate. After processing and calculation, the modified mutation rate and crossover rate change methods can be expressed as follows:

$$
PI_c = \begin{cases} 0.84^{\left(\frac{fit_{\max}-fit_{avg}}{fit_{avg}-fit_{\min}+eps}\right)^2}, & \frac{fit_{\max}-fit_{avg}}{fit_{avg}-fit_{\min}+eps} < 1 \, and \, pop_1 \geq pop_2 \\ otherwise \\ pi_{c1} - \frac{(pi_{c1}-pi_{c2})(fit_{wb}-fit_{\min})}{fit_{\max}-fit_{\min}} \end{cases} \tag{12}
$$

$$
PI_m = \begin{cases} 0.12^{\left(\frac{fit_{\max}-fit_{avg}}{fit_{avg}-fit_{\min}+eps}\right)^2}, & \frac{fit_{\max}-fit_{avg}}{fit_{avg}-fit_{\min}+eps} < 1 \, and \, pop_1 \geq pop_2 \\ otherwise \\ pi_{m1} - \frac{(pi_{m1}-pi_{m2})(fit_{w1}-fit_{\min})}{fit_{\max}-fit_{\min}} \end{cases} \tag{13}
$$

where PI_c and PI_m represent the crossover rate and mutation rate, respectively; pi_{c1} and pi_{c2} are the crossover calculation coefficients with values of 0.9 and 0.6, respectively; pi_{m1} are pi_{m2} the variation calculation coefficients with values of 0.1 and 0.01, respectively; $fit_{\max}$ and $fit_{\min}$ denote the maximum and minimum fitness values of individuals in the population, respectively; fit_{avg} denotes the mean value of the population fitness; fit_{wb} denotes the larger fitness value of the two individuals that are about to cross; fit_{w1} denotes the fitness value of the individual that is about to take part in the mutation; pop_1 and pop_2

denote the number of individuals in the population with higher and lower fitness values than the population mean, respectively; and *eps* is an infinitesimal positive integer.

4. Objective Function

The use of intelligent algorithms to localize and quantify structural damage requires the establishment of a corresponding objective function. The objective function is composed of the dynamic response transfer ratio and modal assurance criterion, which can improve the accuracy and robustness of the identification. Meanwhile, since the dynamic response transfer ratio is independent of the input at the system poles, the modal parameters of the system can be identified from the response data, even if the input is unknown. The dynamic response transfer ratio is combined with the modal assurance criterion [21] to define the following assurance criterion function of the transfer ratio $TFAC(\omega)$, and the dynamic response transfer ratio is combined with the amplitude correlation coefficient [22] to define the following amplitude correlation function of the transfer ratio $TFAC(\omega)$, which can be expressed as

$$TFAC(\omega) = \frac{\left(\boldsymbol{TF}^T(\omega)\boldsymbol{TF}(\omega,\boldsymbol{\alpha})\right)^2}{\left(\boldsymbol{TF}^T(\omega)\boldsymbol{TF}(\omega)\right)\left(\boldsymbol{TF}^T(\omega,\boldsymbol{\alpha})\boldsymbol{TF}(\omega,\boldsymbol{\alpha})\right)} \tag{14}$$

$$TFAL(\omega) = \frac{2 \cdot \left|\boldsymbol{TF}^T(\omega)\boldsymbol{TF}(\omega,\boldsymbol{\alpha})\right|}{\left(\boldsymbol{TF}^T(\omega)\boldsymbol{TF}(\omega)\right) + \left(\boldsymbol{TF}^T(\omega,\boldsymbol{\alpha})\text{TF}(\omega,\boldsymbol{\alpha})\right)} \tag{15}$$

where $\boldsymbol{TF}(\omega)$ is the dynamic response transfer ratio vector measured, and $\boldsymbol{TF}(\omega,\boldsymbol{\alpha})$ is the dynamic response transfer ratio vector calculated based on the finite element modeling theory. The objective function is established based on $TFAC(\omega)$ and $TFAL(\omega)$, which can be expressed as

$$obj_1 = \eta_1 \cdot BJ_1 + \eta_2 \cdot BJ_2 \tag{16}$$

where

$$BJ_1 = \sum_{i=1}^{num}(1 - TFAC(\omega_z)), \ BJ_2 = \sum_{i=1}^{num}(1 - TFAL(\omega_z))$$

and *num* is the number of selected frequency points, $TFAC(\omega_z)$ is the assurance criterion function value of the transfer ratio at the given frequency ω_z, and $TFAL(\omega_z)$ is the amplitude correlation function value of the transfer ratio at the given frequency ω_z. η_1 and η_2 are the different weighting factors.

5. Weighting Factors and Mean Error

Since the assurance criterion function and the amplitude correlation function of the dynamic response transfer ratio have different sensitivities to damage, it is likely that damage will lead to large differences in the values of BJ_1 and BJ_2. This can easily lead to intelligent algorithms taking one part of the objective function as the dominant part of the constrained optimization problem when solving the problem, which, in turn, significantly weakens the role of the other part of the objective function.

In this paper, according to the method described in the literature [23], the weighting factors are calculated and substituted into the objective function so as to weaken the numerical difference between BJ_1 and BJ_2 and make the intelligent algorithm solution more accurate. The specific calculation method is expressed as follows:

$$\eta_1 = \frac{\sum\limits_{na=1}^{nx}\sum\limits_{nb=1}^{ny}\left(BJ_2^{na,nb}\right)/\left(BJ_1^{na,nb}\right)}{\sum\limits_{na=1}^{nx}\sum\limits_{nb=1}^{ny}\left(BJ_2^{na,nb}\right)/\left(BJ_1^{na,nb}\right) + nx^2} \tag{17}$$

where *nx* is the number of units in the structure division, *ny* is the number representing the level of damage grading, $BJ_1^{na,nb}$ and $BJ_2^{na,nb}$ are the values of BJ_1 and BJ_2 for the *na*th unit at damage

level *nb*, respectively. A total of ten levels of damage grading were chosen for this paper, being unit damage levels of 0.1, 0.2, 0.3, 0.4, 0.5, 0.6, 0.7, 0.8, 0.9, and 0.99, in descending order.

In order to evaluate the accuracy of the intelligent algorithm in identifying the damage degree of the preconfigured damage units (the target damage units in this paper refer to the preconfigured damage units in the damage cases) in each damage case in the simulation, the mean error is introduced, which is denoted as

$$Em = \frac{1}{ne} \sum_{\varphi=1}^{ne} \left| \frac{\alpha_\varphi^{\text{th}} - \alpha_\varphi^{\text{re}}}{\alpha_\varphi^{\text{th}}} \right| \times 100\% \tag{18}$$

where $\alpha_\varphi^{\text{th}}$ and $\alpha_\varphi^{\text{re}}$ denote the preconfigured damage degree of the φth preconfigured damage unit and the damage degree identified by the algorithm under a certain case, respectively, and *ne* denotes the number of preconfigured damage units in the case.

6. Numerical Simulation

In order to verify the identification accuracy of the damage identification method based on the RGA and INFO under different levels of noise and different frequency-point spacings, a numerical case study was carried out in MATLAB for simply supported beams and cantilever plates (the damage identification results in this paper are the average values obtained after ten runs). Because it is easy to simulate damage in simply supported beams and cantilever plates, and they have the advantages of a simple structure, strong representation, wide application background, and obvious damage effects, they were taken as research objects. In addition, the mutation rate and crossover rate of the standard GA as a comparison were set to 0.2 and 0.4, respectively, and the number of populations and iterations of the three algorithms were set to 120 and 800, respectively. The acceleration response signal added white noise, which can be expressed as follows:

$$Acc_1 = Acc_0 \cdot (1 + noi \cdot rdn) \tag{19}$$

where Acc_1 and Acc_0 are the acceleration response signals before and after the noise interference, and *noi* is the noise level, which is a standard normally distributed random number.

6.1. Simulation of a Simply Supported Beam

The model of the simply supported beam is shown in Figure 4. Its one section is fixed, and the bottom end of the other section is connected to a movable hinge support. The beam has an axial length of 1.2 m and is divided into 12 units, and the cross-section is a rectangle with a width of 0.05 m and a height of 0.015 m. The modulus of elasticity of the material is set to 2.061011 Pa, while Poisson's ratio is 0.3, and the density is 7850 kg/m^3. The first five orders of the nature frequencies of the model are 24.19 Hz, 96.66 Hz, 217.07 Hz, 384.76 Hz, and 598.42 Hz.
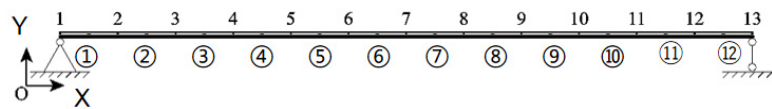

Figure 4. Numerical simulation model of the simply supported beam.

Two damage cases, as shown in Table 1, are set up in the model of the simply supported beam. The numbers after "/" in Table 1 and the subsequent tables represent the degree of damage of the unit.

Table 1. Damage case settings for the simply supported beam.

Damage Case Number	Damage Unit Number/Degree of Damage%
1	5/13%, 9/9%
2	3/19%, 6/15%, 10/15%

In the simulation, single-point excitation is applied to node 3 of the model, and the Y-direction transfer ratio of each node substituted into the objective function is calculated with the Y-direction acceleration response of node 2 as a reference. The frequency range of the objective function is taken from 1 Hz to 400 Hz (including the first four orders of the nature frequencies of the model), and 400 frequency points are taken at equal intervals of 1 Hz in the frequency range.

The three intelligent algorithms were used to identify the damage in the two damage cases of the simply supported beam in Table 1 in the absence of noise, and the results of the damage identification in each beam unit in Case 1 and Case 2 are shown in Figures 5 and 6, and the results of the identification of the target damage unit are shown in Table 2.
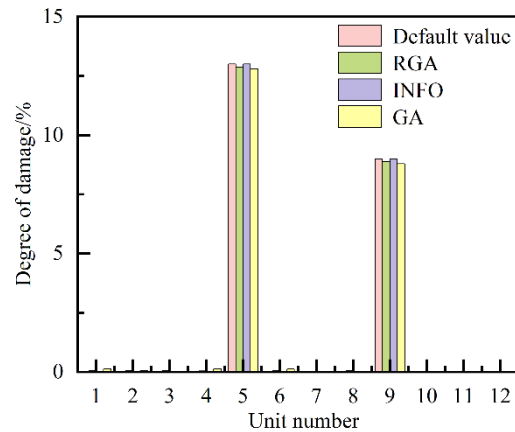
Figure 5. Damage identification results of each beam unit in Case 1 (no noise).
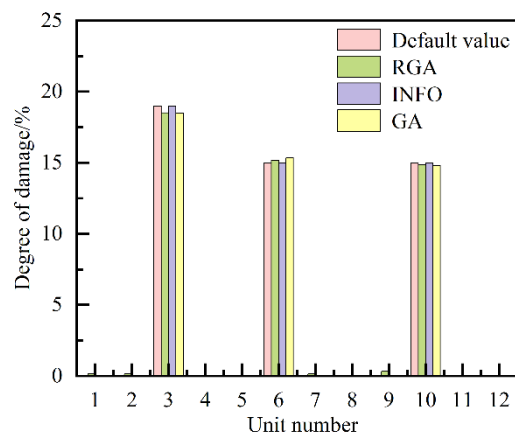
Figure 6. Damage identification results of each beam unit in Case 2 (no noise).

Table 2. Identification results for the target damage units for the simply supported beam (no noise).

Damage Case Number	Damage Unit Number/Degree of Damage%		
	GA	RGA	INFO
1	5/12.80%, 9/8.79%	5/12.86%, 9/8.90%	5/13.00%, 9/9.00%
2	3/18.51%, 6/15.34%, 10/14.82%	3/18.52%, 6/15.19%, 10/14.85%	3/19.00%, 6/15.00%, 10/15.00%

It can be observed from Figures 5 and 6 that the three algorithms can accurately locate the damage in Case 1 and Case 2 without noise interference, and none of the three algorithms have obvious misjudgment units.

Further analysis of Table 2 shows that the mean errors of the target damage units identified by GA and RGA in Case 1 are 1.94% and 1.09%, while in Case 2, they are 2.02%

and 1.60%, respectively, while INFO has the highest identification accuracy without obvious errors for the two cases.

However, the measured response data will inevitably be affected by different levels of noise in practical engineering applications. Two levels of noise (1% and 3%) were added to Case 1, and the damage identification results for each beam unit under the influence of these different levels of noise are shown in Figures 7 and 8, respectively.
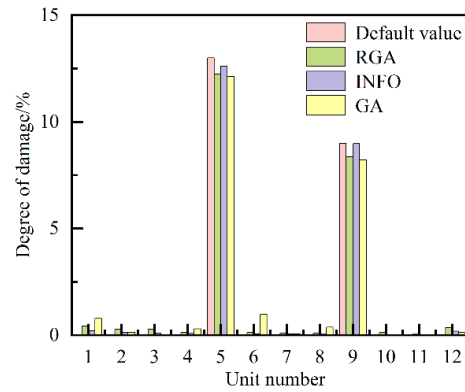

Figure 7. Damage identification results for each beam unit under 1% noise (Case 1).
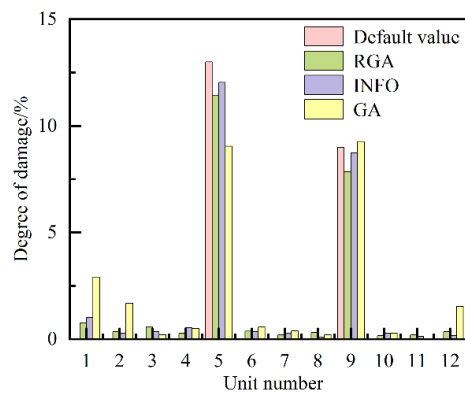
Figure 8. Damage identification results for each beam unit under 3% noise (Case 1).

From Figures 7 and 8, it can be seen that all the three algorithms accurately identify the damage location in the simply supported beam under the influence of 1% as well as 3% noise, but only under the influence of 3% noise is there a significant misjudgment by the GA in the damage identification of the simply supported beam model at units 1, 2 and 12.

Figure 9 shows the damage identification results for each unit when 10% noise was added to Case 1.
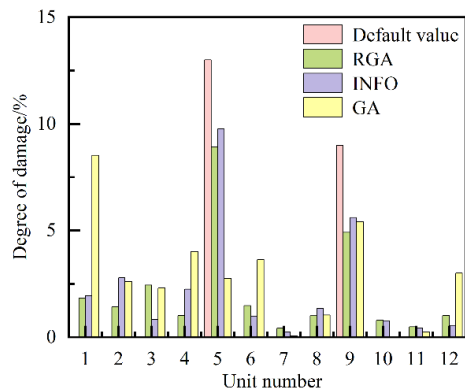
Figure 9. Damage identification results for each beam unit under 10% noise (Case 1).

From Figure 9, it can be seen that under the influence of 10% noise, the three algorithms' damage identification results are significantly worse compared with ones under the influence of 1% and 3% noise, and there are many obvious misjudgment units; GA is relatively more affected by this level of noise, while the other two algorithms' damage identification results are better than that of GA.

The identification results under the influence of 1%, 3%, and 10% noise are shown in Table 3.

Table 3. Identification results of the target damage units in the simply supported beam under three different levels of noise (Case 1).

Noise Level/%	Damage Unit Number/Degree of Damage%		
	GA	RGA	INFO
1	5/12.13%, 9/8.215%	5/12.23%, 9/8.36%	5/12.61%, 9/8.97%
3	5/9.04%, 9/9.26%	5/11.44%, 9/7.85%	5/12.03%, 9/8.74%
10	5/2.75%, 9/5.42%	5/8.91%, 9/4.92%	5/9.765, 9/5.61%

Table 3 (Case 1) shows that under the influence of 1%, 3%, and 10% noise, the mean errors of the target damage units identified by the GA are 7.74%, 16.68%, and 59.31%, while those identified by the RGA are 6.52%, 12.39%, and 38.40% and those identified by INFO are 1.67%, 5.18%, and 31.29%, respectively. It can be seen that INFO has the highest accuracy while RGA has the second highest, and GA has the lowest accuracy in identifying the damage degree of the target unit. The mean error of the three algorithms in identifying the damage in the target unit in Case 1 increases significantly when the results of the 10% noise are compared with those with 1% and 3% noise, which is mainly due to the fact that too high a level of noise seriously affects the transfer ratio obtained and, ultimately, results in the failure to obtain a more accurate damage degree of the target unit, even if the value of the objective function converges more closely to the global optimum.

Subsequently, the same noise in Case 1 was added to Case 2, and the results of the damage identification of each unit under the influence of the three different levels of noise are shown in Figure 10, Figure 11, and Figure 12, respectively.
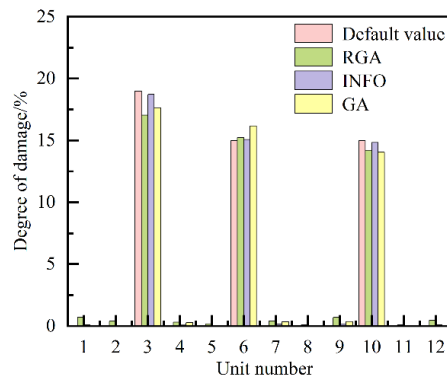

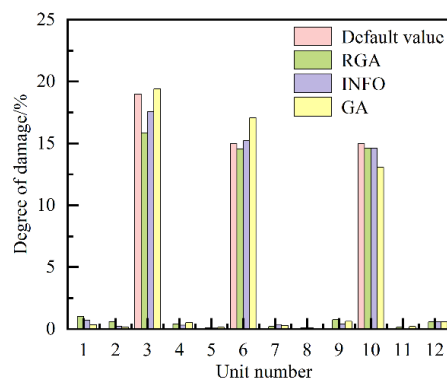**Figure 10.** Damage identification results for each beam unit under 1% noise (Case 2).

Figure 11. Damage identification results for each beam unit under 3% noise (Case 2).
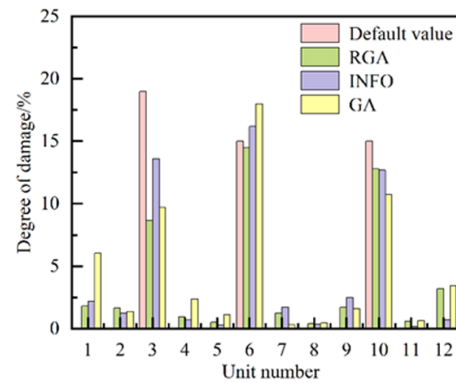
Figure 12. Damage identification results for each beam unit under 10% noise (Case 2).

From Figures 10 and 11, it can be seen that the three algorithms can accurately identify the damage location in the simply supported beam under the influence of 1% and 3% noise. Compared with the aforementioned Case 1 (simply supported beam), under the influence of 3% noise, damage identification using the GA does not result in obvious misjudgment units, mainly because the damage degree of the damage unit in Case 2 is larger, and the identification is not easily affected by the noise.

Further studies were carried out by adding 10% noise to the Case 2 (simply supported beam), and the results of the damage identification for each beam unit are shown in Figure 12.

From Figures 10–12, it can be seen that there is the same pattern as for Case 1. But under the influence of 3% noise, the results are not the same as for Case 1; damage identification using the GA does not appear to present obvious misjudgment units, mainly because the damage degree of the damage unit in Case 2 is larger, and the identification results are not easily affected by the noise.

The results of identifying the target damage units (Case 2) under the influence of 1%, 3%, and 10% noise are shown in Table 4.

Table 4. Identification results for the target damage units of the simply supported beam under three different levels of noise (Case 2).

Noise Level/%	Damage Unit Number/Degree of Damage%		
	GA	RGA	INFO
1	3/17.65%, 6/16.18%, 10/14.05%	3/17.04%, 6/15.25%, 10/14.21%	3/18.72%, 6/15.07%, 10/14.84%
3	3/19.42%, 6/17.08%, 10/13.06%	3/15.87%, 6/14.56%, 10/14.62%	3/17.57%, 6/15.22%, 10/14.63%
10	3/9.71%, 6/18.01%, 10/10.75%	3/8.69%, 6/14.51%, 10/12.79%	3/13.58%, 6/16.17%, 10/12.69%

Table 4 (Case 2) shows that under the influence of 1%, 3%, and 10% noise, the mean errors of the target damage units identified by the GA are 7.10%, 9.67%, and 32.43%, while they are 5.75%, 7.31%, and 24.09% by the RGA, and 1.00%, 3.82%, and 17.24% by INFO, respectively. Comparing the mean errors, it can be seen that INFO has the highest accuracy in identifying the damage degree of the target unit, while RGA has the second highest accuracy, and GA has the lowest accuracy.

In the aforementioned simulation, more frequency points in a larger frequency range were used, leading to increased computation. So, reducing the frequency points was considered. Keeping the frequency range from 1 Hz to 400 Hz unchanged, the following three scenarios were simulated for Case 2: (1) Taking points at equal intervals of 2 Hz for a total of 200 frequency points. (2) Taking points at equal intervals of 4 Hz for a total of 100 frequency points. (3) Taking points at equal intervals of 8 Hz for a total of 50 frequency points. The damage identification results from adding 3% noise are shown in Figure 13 and Table 5.
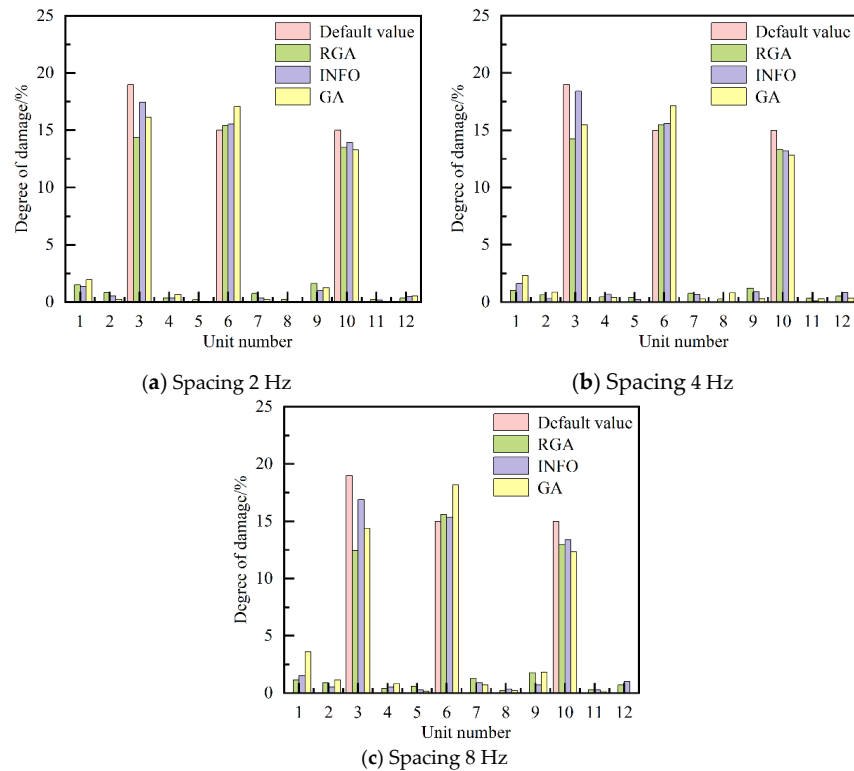
(**a**) Spacing 2 Hz

(**b**) Spacing 4 Hz

(**c**) Spacing 8 Hz

Figure 13. Damage identification results for each beam unit with different frequency points.

Table 5. Identification results with different frequency-point spacings (Case 2).

Taking Point Spacing/Hz	Damage Unit Number/Degree of Damage%		
	GA	RGA	INFO
2	3/16.13%, 6/17.07%, 10/13.29%	3/14.38%, 6/15.42%, 10/13.51%	3/17.47%, 6/15.54%, 10/13.93%
4	3/15.46%, 6/17.16%, 10/12.85%	3/14.24%, 6/15.50%, 10/13.35%	3/18.40%, 6/15.62%, 10/13.18%
8	3/14.39%, 6/18.20%, 10/12.34%	3/12.45%, 6/15.61%, 10/12.97%	3/16.89%, 6/15.33%, 10/13.37%

From Figure 13, it can be observed that under the influence of the same noise, the three algorithms obtained slightly worse damage identification results for each beam unit at the 2 Hz spacing than at the 1 Hz spacing (aforementioned results in Figure 11), but there is no obvious difference in the identification results when comparing the 4 Hz and 8 Hz spacings.

Table 5 shows that under the influence of the same noise, the mean errors of the target damage identified by the three methods are 13.44%, 12.35%, and 6.26% at a 2 Hz spacing, 15.79%, 13.13%, and 6.47% at a 4 Hz spacing, and 21.11%, 17.36%, and 8.06% at an 8 Hz spacing, respectively. The identification accuracy for the three algorithms becomes lower and lower with the gradual increase in the taking-point spacing within the same frequency range, and the identification accuracy of INFO is the highest, with the second highest identification accuracy for the RGA, and the lowest identification accuracy for the GA.

6.2. Simulation of the Cantilever Plate

The cantilever plate model is shown in Figure 14, with its left end fixed. The length, width, and thickness of the cantilever plate are 0.5 m, 0.3 m, and 0.004 m, respectively; the density of the structural material is 7850 kg/m^3; the modulus of elasticity is 2.06×10^{11} Pa; the Poisson ratio is 0.3; and it is divided into 15 plate-shell units, with the length and width of each unit being 0.1 m, and the left edge of the plate is fixed. The first five orders of its nature frequencies are 13.61 Hz, 50.21 Hz, 85.46 Hz, 167.02 Hz, and 236.78 Hz. The numbers above the nodes of the units are the node numbers, and the numbers inside the circles are the cell unit numbers.
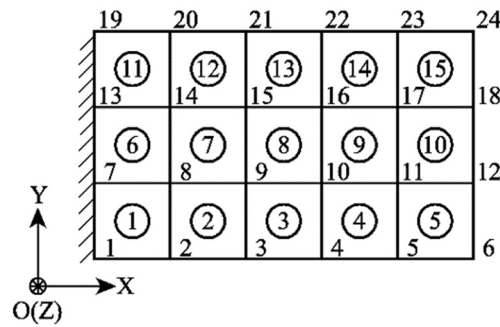
Figure 14. Cantilever plate model.

The cantilever plate model is set up with two damage cases, as shown in Table 6.

Table 6. Damage case settings for the cantilever plate.

Damage Case Number	Damage Unit Number/Degree of Damage %
3	2/18%, 10/13%
4	4/12%, 7/16%, 12/14%

In the simulation, a single-point excitation is applied to node 18 of the cantilever plate model, and the Z-direction transfer ratio of each node substituted into the objective function is calculated, with the Z-direction acceleration response of node 20 as a reference. The frequency range of the objective function is taken from 11 Hz to 240 Hz (including the first five orders of the nature frequency of the model), and 230 frequency points are taken at equal intervals of 1 Hz.

The three intelligent algorithms were used to identify the damage in the two damage cases using the cantilever plate without adding noise, as in Table 6. The results of the damage identification in Case 3 and Case 4 are shown in Figures 15 and 16 and Table 7.
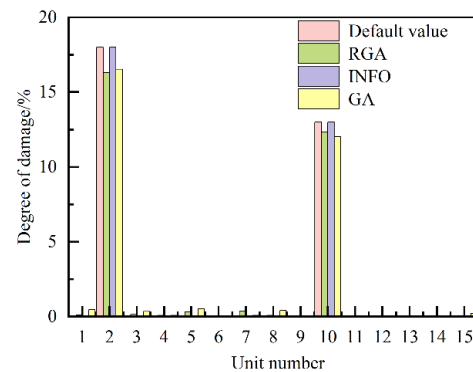
Figure 15. Damage identification results for each plate unit in Case 3 (no noise).
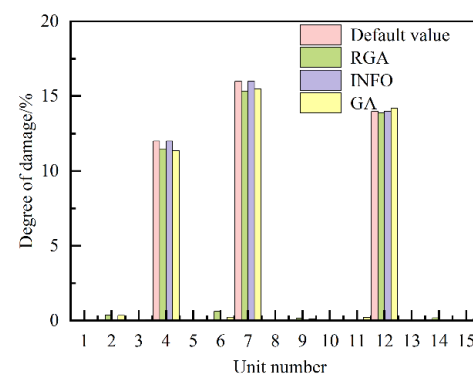

Figure 16. Damage identification results for each plate unit in Case 4 (no noise).

Table 7. Identification results for the target damage units of the cantilever plate (no noise).

Damage Case Number	Damage Unit Number/Degree of Damage%		
	GA	RGA	INFO
3	2/16.54%, 10/12.02%	2/16.32%, 10/12.35%	2/18.00%, 10/13.00%
4	4/11.36%, 7/15.47%, 12/14.20%	4/11.48%, 7/15.35%, 12/13.87%	4/12.00%, 7/16.00%, 12/14.00%

It can be observed from Figures 15 and 16 that the three intelligent algorithms can accurately localize the two damage sites in Case 3 and the three damage sites in Case 4 without any obvious misjudgment unit in the absence of noise interference.

Table 7 shows that the mean errors of the target damage units identified by the GA and the RGA in Case 3 are 7.82% and 7.38%, and 3.36% and 3.11% in Case 4, respectively, whereas there are significant identification errors in both cases for INFO.

Then, 1%, 3%, and 10% noise was added to the cantilever plate damage in Case 3. The results of damage identification under the influence of the three different levels of noise are shown in Figure 17, Figure 18, and Figure 19, respectively, and summarized in Table 8.
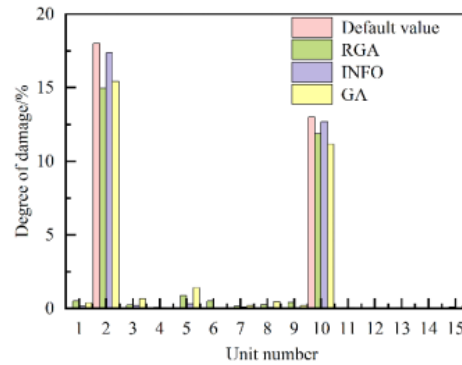

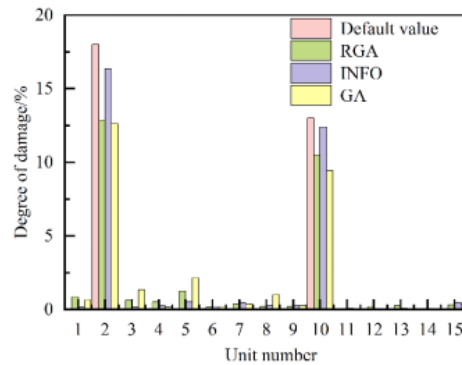**Figure 17.** Damage identification results for each plate unit under 1% noise (Case 3).

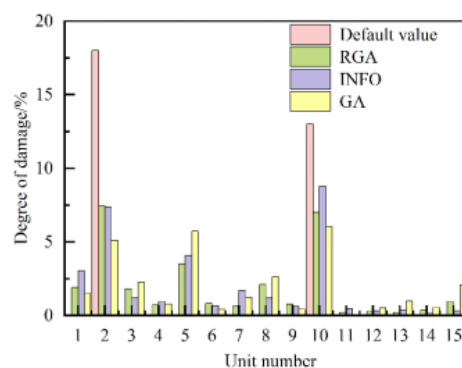**Figure 18.** Damage identification results for each plate unit under 3% noise (Case 3).

Figure 19. Damage identification results for each plate unit under 10% noise (Case 3).

Table 8. Identification results for the target damage units of the cantilever plate under three different levels of noise (Case 3).

Noise Level/%	Damage Unit Number/Degree of Damage%		
	GA	RGA	INFO
1	2/15.43%, 10/11.17%	2/14.94%, 10/11.89%	2/17.37%, 10/12.70%
3	2/12.62%, 10/9.44%	2/12.87%, 10/10.46%	2/16.37%, 10/12.41%
10	2/5.12%, 10/6.06%	2/7.45%, 10/7.01%	2#/7.38%, 10/8.80%

From Figures 17–19, it can be seen that under the influence of 1% and 3% noise, the GA, RGA and INFO can accurately locate the damage position in the cantilever plate; of these, INFO has the best damage identification results without significant misjudgment units, while more significant misjudgment units are found for both the GA and the RGA. However, under the influence of 10% noise, there are many obvious misjudgment units for the three methods.

Table 8 (Case 3) shows that under the influence of 1%, 3%, and 10% noise, the mean errors of the target damage units identified by the GA are 14.18%, 28.64%, and 62.47%, 12.77%, 24.02%, and 52.34% by the RGA, and 2.90%, 6.80%, and 45.65% by INFO, respectively. It can be seen that INFO has the highest accuracy, the RGA has the second highest accuracy, and the GA has the lowest accuracy.

The results of damage identification after adding 1%, 3%, and 10% noise to Case 4 are shown in Figure 20, Figure 21, and Figure 22, respectively, and summarized in Table 9.
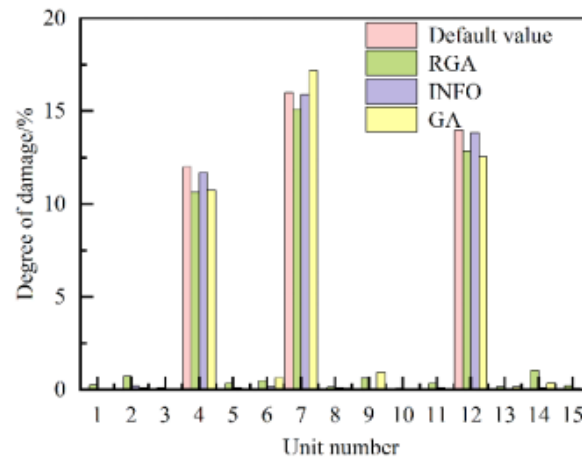

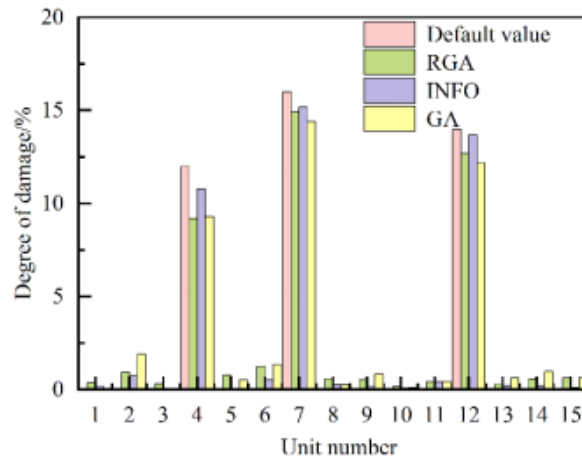**Figure 20.** Damage identification results for each plate unit under 1% noise (Case 4).

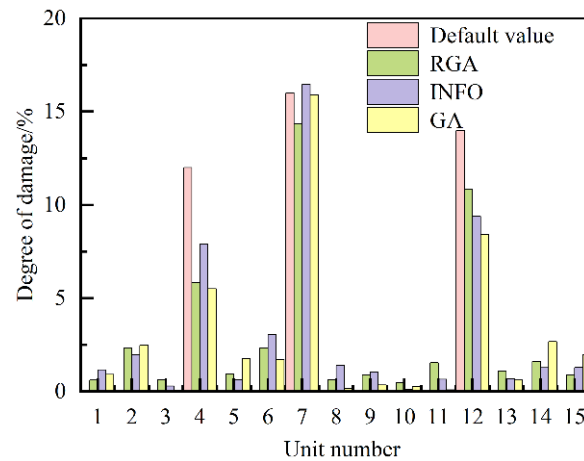**Figure 21.** Damage identification results for each plate unit under 3% noise (Case 4).

Figure 22. Damage identification results for each plate unit under 10% noise (Case 4).

Table 9. Identification results for the target damage units of the cantilever plate under three different levels of noise (Case 4).

Noise Level/%	Damage Unit Number/Degree of Damage%		
	GA	RGA	INFO
1	4/10.73%, 7/17.18%, 12/12.54%	4/10.65%, 7/15.09%, 12/12.85%	4/11.70%, 7/15.91%, 12/13.83%
3	4/9.29%, 7/14.41%, 12/12.16%	4/9.20%, 7/14.91%, 12/12.68%	4/10.80%, 7/15.18%, 12/13.69%
10	45.51%, 7/15.89%, 12/8.42%	4/5.83%, 7/14.34%, 12/10.82%	4/7.91%, 7/16.46%, 12/9.38%

From Figures 20–22, it is observed that the GA, RGA and INFO are able to accurately locate the damage position in the cantilever plate (Case 4) under 1% as well as 3% noise influence. Under 3% noise, the GA and RGA have more significant misjudgments at units 2 and 6, and INFO has significant misjudgment at unit 2, while under the influence of 10% noise, there are many obvious misjudgment units for the three methods.

Table 9 (Case 4) shows that under the influence of 1%, 3% and 10% noise, the mean errors of the target damage units identified by GA are 9.46%, 15.22% and 31.54%, 8.38%, 13.19%, and 28.17% by RGA, and 1.40%, 5.78%, and 23.32% by INFO, respectively. It can be seen that INFO has the highest accuracy in identifying the damage degree of the target unit, the RGA has the second highest accuracy, and the GA has the lowest accuracy.

Keeping the frequency range from 11 Hz to 240 Hz unchanged, the following three scenarios were simulated for Case 4 of the cantilever plate (adding 3% noise): (1) Taking points at equal intervals of 2 Hz for a total of 115 frequency points. (2) Taking points at equal intervals of 4 Hz for a total of 58 frequency points. (3) Taking points at equal intervals of 8 Hz for a total of 29 frequency points. The damage identification results are shown in Figure 23, and the target damage unit identification results are shown in Table 10.

Table 10. Identification results for the target damage units of the cantilever plate with different frequency-point spacings (Case 4).

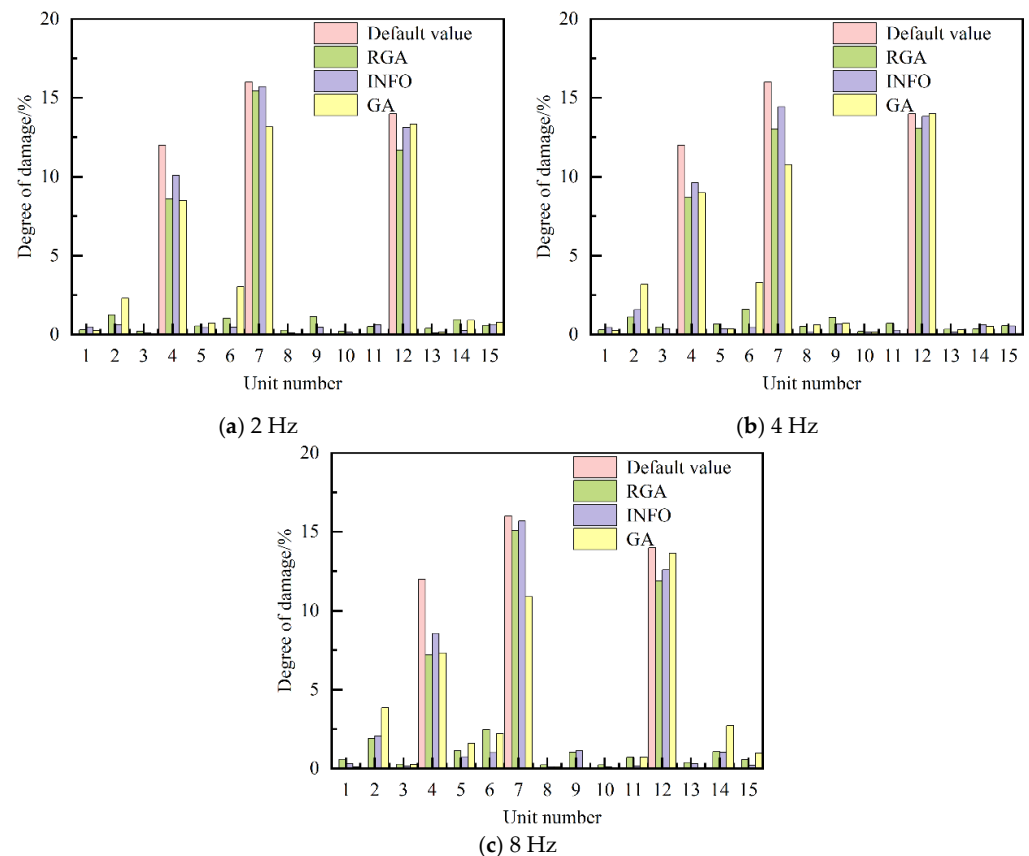| Noise Level/%	Damage Unit Number/Degree of Damage%		
	GA	RGA	INFO
2	4/8.48%, 7/13.16%, 12/13.31%	4/8.62%, 7/15.45%, 12/11.67%	4/10.10%, 7/15.71%, 12/13.13%
4	4/8.99%, 7/10.78%, 12/14.01%	4/8.68%, 7/13.02%, 12/13.06%	4/9.62%, 7/14.43%, 12/13.82%
8	4/7.34%, 7/10.89%, 12/13.62%	4/7.21%, 7/15.08%, 12/11.90%	4/8.57%, 7/15.68%, 12/12.59%

(a) 2 Hz

(b) 4 Hz

(c) 8 Hz

Figure 23. Damage identification results for each plate unit with different frequency-point spacings.

From Figure 23, it can be observed that under the influence of the same noise, the three algorithms can identify the damage location of the cantilever plate for three kinds of taking-point spacings, and the three algorithms obtained slightly worse damage identification results for each plate unit at the 2 Hz spacing than the results of the aforementioned 1 Hz spacing (Figure 21), but there is no obvious advantage in comparison with the identification results obtained at the 4 Hz spacing, while identification results for the 4 Hz spacing are better than those for the 8 Hz spacing.

Table 10 shows that under the influence of the same noise, when equally spaced at 2 Hz, the mean errors of the target damage units identified for the GA, RGA, and INFO are 17.34%, 16.08%, and 7.95%, while they are 19.26%, 17.67%, and 10.31% when equally spaced at 4Hz, and 24.50%, 20.22%, and 13.55%, when equally spaced at 8Hz, respectively. It can be seen that the identification accuracy of the three algorithms becomes lower and lower with the gradual increase in taking-point spacing within the same frequency range. With the same taking-point spacing, INFO has the highest identification accuracy, RGA has the second highest identification accuracy, and GA has the worst identification accuracy.

7. Conclusions

This paper introduces and evaluates a novel structural damage identification method based on INFO, a sophisticated optimization technique, and compares its performance with the RGA (which is obtained by improving the mutation operator, crossover rate, and mutation rate) and the traditional GA. The paper employs a dynamic response transfer-ratio-based objective function, which is optimized using INFO, the RGA, and the GA to identify damage in numerical models of a simply supported beam and a cantilever plate. By making a comparative analysis of the simulation results, the following are concluded:

1. For most of the same cases, INFO has the highest damage identification accuracy, the RGA has the second highest identification accuracy, and the GA has the lowest

2. Under the same case, as the noise level gradually increases, the accuracy of damage identification by the algorithms will gradually become lower. For INFO, under the influence of 1% and 3% noise levels, the identification error of the damage degree of the target unit is below 3% and 8%, while under the influence of a 10% noise level, the error is above 30%.

3. Within the same frequency range and with a gradual increase in the frequency-point spacing, the accuracy of the algorithm damage identification gradually decreases, but there is no significant increase in the error for the part of the identification results obtained after the increase in the spacing of the point spacing, and the error is still within an acceptable range.

In conclusion, the INFO algorithm has emerged as a powerful tool for structural damage identification, offering a balance of accuracy, robustness, and efficiency. Its performance surpasses that of the RGA and the GA, making it a promising candidate for further research and practical implementation in structural health monitoring systems. Future work may focus on applying the INFO algorithm to more complex structures, exploring its scalability, and integrating it with other damage identification techniques to enhance its applicability in real-world scenarios.

Author Contributions: Conceptualization, J.M. and Z.Y.; methodology, Z.Y. and J.M.; software, Z.Y. and J.M.; writing—Z.Y. and J.M.; writing—review and editing, Z.Y., J.M. and Y.Q.; supervision, J.M. and Y.Q. All authors have read and agreed to the published version of the manuscript.

Institutional Review Board Statement: Not applicable.

Informed Consent Statement: Not applicable.

Data Availability Statement: The data presented in this study are available on request from the corresponding author due to policy decisions of their respective agencies.

Conflicts of Interest: The authors declare no conflict of interest.

References

1. Abubakar, I.; Stagg, H.R.; Cohen, T.; Mangtani, P.; Rodrigues, L.C.; Pimpin, L.; Watson, J.M.; Squire, S.B.; Zumla, A. Controversies and Unresolved Issues in Tuberculosis Prevention and Control: A Low-Burden-Country Perspective. *J. Infect. Dis.* **2012**, *205* (Suppl. 2), S293–S300. [CrossRef] [PubMed]

2. Huang, M.; Chaoyue, Q.I.; Cheng, S. Damage identification of the benchmark frame based on an improved cuckoo search. *J. Vib. Shock* **2018**, *27*, 158–163.

3. Hoseini Vaez, S.R.; Fallah, N. Damage detection of thin plates using GA-PSO algorithm based on modal data. *Arab. J. Sci. Eng.* **2017**, *42*, 1251–1263. [CrossRef]

4. Huang, M.; Wan, Z.; Cheng, X.; Xu, Z.; Lei, Y.; Pan, D. Two-stage damage identification method based on fractal theory and whale optimization algorithm. *Adv. Struct. Eng.* **2021**, *25*, 1026–1058. [CrossRef]

5. Mohan, S.C.; Maiti, D.K.; Maity, D. Structural damage assessment using FRF employing particle swarm optimization. *Appl. Math. Comput.* **2013**, *219*, 10387–10400. [CrossRef]

6. Miguel, L.F.F.; Lopez, R.H.; Miguel, L.F.F. A hybrid approach for damage detection of structures under operational conditions. *J. Sound Vib.* **2013**, *332*, 4241–4260. [CrossRef]

7. Ding, Z.H.; Huang, M.; Lu, Z.R. Structural damage detection using artificial bee colony algorithm with hybrid search strategy. *Swarm Evol. Comput.* **2016**, *28*, 1–13. [CrossRef]

8. Pan, C.D.; Yu, L.; Chen, Z.P.; Luo, W.F.; Liu, H.L. A hybrid self-adaptive Firefly-Nelder-Mead algorithm for structural damage detection. *Smart Struct. Syst.* **2016**, *17*, 957–980. [CrossRef]

9. Chen, Z.; Yu, L. A new structural damage detection strategy of hybrid PSO with Monte Carlo simulations and experimental verifications. *Measurement* **2018**, *122*, 658–669. [CrossRef]

10. Gomes, G.F.; da Cunha, S.S.; Ancelotti, A.C. A sunflower optimization (SFO) algorithm applied to damage identification on laminated composite plates. *Eng. Comput.* **2019**, *35*, 619–626. [CrossRef]

11. Alkayem, N.F.; Cao, M.; Ragulskis, M. Damage localization in irregular shape structures using intelligent FE model updating approach with a new hybrid objective function and social swarm algorithm. *Appl. Soft Comput.* **2019**, *83*, 105604. [CrossRef]
12. Huang, M.; Li, X.; Lei, Y.; Gu, J. Structural damage identification based on modal frequency strain energy assurance criterion and flexibility using enhanced Moth-Flame optimization. *Structures* **2020**, *28*, 1119–1136. [CrossRef]
13. Minh, H.L.; Khatir, S.; Wahab, M.A.; Cuong-Le, T. An Enhancing Particle Swarm Optimization Algorithm (EHVPSO) for damage identification in 3D transmission tower. *Eng. Struct.* **2021**, *242*, 112412. [CrossRef]
14. Li, X.L.; Serra, R.; Olivier, J. A multi-component PSO algorithm with leader learning mechanism for structural damage detection. *Appl. Soft Comput.* **2022**, *116*, 108315. [CrossRef]
15. YiFei, L.; Minh, H.L.; Khatir, S.; Sang-To, T.; Cuong-Le, T.; MaoSen, C.; Wahab, M.A. Structure damage identification in dams using sparse polynomial chaos expansion combined with hybrid K-means clustering optimizer and genetic algorithm. *Eng. Struct.* **2023**, *283*, 115891. [CrossRef]
16. Sang-To, T.; Le-Minh, H.; Wahab, M.A.; Thanh, C.L. A new metaheuristic algorithm: Shrimp and Goby association search algorithm and its application for damage identification in large-scale and complex structures. *Adv. Eng. Softw.* **2023**, *176*, 103363. [CrossRef]
17. Shirazi, M.I.; Khatir, S.; Benaissa, B.; Mirjalili, S.; Wahab, M.A. Damage assessment in laminated composite plates using modal strain energy and YUKI-ANN algorithm. *Compos. Struct.* **2023**, *303*, 116272.
18. Holland, J. Genetic algorithms. *Sci. Am.* **1992**, *267*, 66–73. [CrossRef]
19. Ahmadianfar, I.; Heidari, A.A.; Noshadian, S.; Chen, H.; Gandomi, A.H. INFO: An efficient optimization algorithm based on weighted mean of vectors. *Expert Syst. Appl.* **2022**, *195*, 116516. [CrossRef]
20. Shabir, S.; Singla, R. A comparative study of genetic algorithm and the particle swarm optimization. *Int. J. Electr. Eng* **2016**, *9*, 215–223.
21. Allemang, R.J. The Modal Assurance Criterion (MAC): Twenty years of use and abuse. *J. Sound Vib.* **2003**, *37*, 14–23.
22. Tong, Z.; Zhang, Y.; Shen, R. Submarine finite element model updating method based on frequency response functions of vibration. *J. Shanghai Jiaotong Univ.* **2005**, *39*, 111–114.
23. Lv, H.; Feng, Z.; Wang, X.; Zhou, W.; Chen, B. Structural damage identification based on hybrid whale annealing algorithm and sparse regularization. *J. Vib. Shock* **2021**, *40*, 85–91.